Liquid Crystals
Publication details, including instructions for authors and subscription information:
http://www.informaworld.com/smpp/title~content=t713926090

Synthesis and characterization of new ferroelectric liquid crystals containing a (2*S*)-2-[6-(4-hydroxybiphenyl-4'-carbonyloxy)-2'- naphthyl] propionate mesogenic group and oligo(oxyethylene) spacers

Ging-Ho Hsiue[ab]; Cheng-Pei Hwang[a]; Jr-Hong Chen[a]; Rong-Chi Chang[a]
[a] Department of Chemical Engineering, National Tsing Hua University, Taiwan [b] Department of Chemical Engineering, National Chung Hsing University, Taiwan, China

To cite this Article Hsiue, Ging-Ho , Hwang, Cheng-Pei , Chen, Jr-Hong and Chang, Rong-Chi(1996) 'Synthesis and characterization of new ferroelectric liquid crystals containing a (2*S*)-2-[6-(4-hydroxybiphenyl-4'-carbonyloxy)-2'-naphthyl] propionate mesogenic group and oligo(oxyethylene) spacers', Liquid Crystals, 20: 1, 45 — 57
To link to this Article: DOI: 10.1080/02678299608032026
URL: http://dx.doi.org/10.1080/02678299608032026

LIQUID CRYSTALS, 1996, VOL. 20, NO. 1, 45–57

Synthesis and characterization of new ferroelectric liquid crystals containing a (2*S*)-2-[6-(4-hydroxybiphenyl-4′-carbonyloxy)-2′-naphthyl]propionate mesogenic group and oligo(oxyethylene) spacers

by GING-HO HSIUE†‡*, CHENG-PEI HWANG†, JR-HONG CHEN† and RONG-CHI CHANG†

†Department of Chemical Engineering, National Tsing Hua University, Hsinchu, Taiwan

‡Department of Chemical Engineering, National Chung Hsing University, Taichung, Taiwan, China

(*Received 30 June 1995; accepted 26 July 1995*)

Three series of ferroelectric liquid crystals containing a (2*S*)-2-(6-(4-hydroxybiphenyl-4′-carbonyloxy)-2′-naphthyl)propionate mesogenic group and oligo(oxyethylene) spacers were synthesized. These obtained liquid crystal compounds were characterized by NMR, differential scanning calorimetry (DSC), optical polarized microscopy (POM), and X-ray powder diffraction measurements. Some of these materials containing four phenyl rings of ester cores (i.e. –Ph–Ph–COO–naph–) and chiral heptyl tail exhibited a rich mesomorphic behaviour, a blue phase (BP), a cholesteric phase (Ch), a smectic A (S_A), a twist grain boundary A (TGB_A), and a chiral smectic C (S_C^*) phase. Another series containing four phenyl rings of ester cores and chiral butyl and pentyl chain tails revealed only a S_A phase and a S_C^* phase. Moreover, a crystal E phase was observed in the short spacer chain ($n=0$ or 1) homologues of three series of compounds. Also, the mesomorphism properties were discussed as a function of spacer units, numbers of aromatic rings of core, and different terminal asymmetric moieties.

1. Introduction

The discovery of ferroelectricity in the S_C^* phase by Meyer *et al.* [1] and the proposal of electro-optical devices using FLCs by Clark and Lagerwall in 1980 [2], have led to extensive studies on FLC materials because of their rapid switching time, and memory effect toward an applied electric field [3]. These characteristics make them highly desirable for electro-optical applications, for example, display and light valve devices. The capability of FLC materials to exhibit a smectic phase over a wide temperature range, including room temperature, would be advantageous in FLC display devices. Moreover, the liquid crystalline material must possess a large spontaneous polarization, so that a FLC related device can be operated at a reduced driving voltage. These properties are influenced by the molecular structure of the liquid crystalline compounds. Consequently, it is of interest to synthesize ferroelectric liquid crystal compounds and compositions which exhibit favourable spontaneous polarization values and their smectic character over a wide range of temperatures, especially at room temperature.

Besides low molar mass FLCs, several side chain liquid crystalline polymers (LCPs) exhibiting a chiral smectic C mesophase have been reported [4–7]. Ferroelectric properties, for example, spontaneous polarization in these polymers, have also been provided in some cases [4–7]. As a part of the research programme dedicated to the development of high efficiency FLC materials, we have designed and synthesized some novel low molar mass FLCs and ferroelectric side chain liquid crystalline polymers [8–14]. They exhibit a broad temperature range of chiral smectic C phases and satisfactory electro-optical properties [10].

In this study, three new series of FLCs are synthesized and characterized. These materials contain oligo(oxyethylene) spacers, a (2*S*)-2-(6-(4-hydroxybiphenyl-4′-carbonyloxy)-2′-naphthyl)propionate mesogenic group, and various chiral moieties, including (*S*)-2-methyl-1-butyl, (*R*)-1-methylheptyl, and (2*S*,3*S*)-2-chloro-3-methylpentyl. The influences of spacer units and different chiral tails on the formation of mesophases are also discussed.

*Author for correspondence.

0267–8292/96 $12·00

The new series have the general formulae:

Series **I**

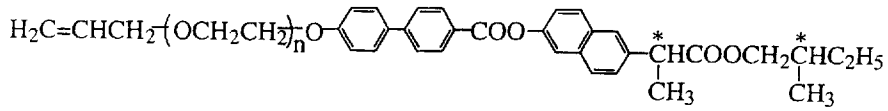

MD*n*2NA (n= 0, 1, 2, 3)

Series **II**

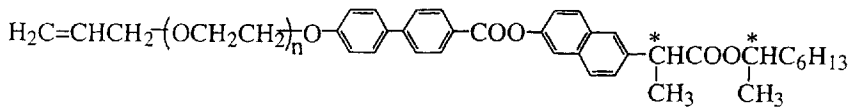

MD*n*2NB (n= 0, 1, 2, 3)

Series **III**

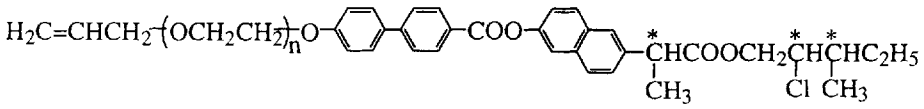

MD*n*2NC (n= 0, 1, 2, 3)

2. Synthesis

The compounds of series MD*n*2NA, MD*n*2NB, and MD*n*2NC were prepared following the scheme. Synthesis details of the above reactions are described in the experimental section.

3. Results and discussion

The phase sequences and the corresponding transition temperatures for these new series are listed in table 1 and figure 1 (*a*)–(*c*).

3.1. *Optical microscopy*

3.1.1. *Series MDn2NA*

Four members of this series contain a (*S*)-2-methyl-1-butyl chiral moiety, oxyethylene unit chains, and a (2*S*)-2-(6-(4-hydroxybiphenyl-4′-carbonyloxy)-2′-naphthyl) propionate mesogenic group. The first derivative having no oxyethylene unit (n=0) exhibits an enantiotropic crystal E phase and a smectic A phase. The other three derivatives (n=1–3) display an isotropic (I)–smectic A (S_A)–chiral smectic C (S_C^*)–crystalline (Cr) liquid crystalline phase sequence. The S_C^* phase in these three derivatives is monotropic. Upon cooling from isotropic liquid, a focal-conic or a homeotropic texture (see figure 2 (*a*)) grew gradually during the formation of S_A phase. After further cooling from the focal-conic or the homeotropic S_A phase, the ferroelectric S_C^* phase was observed in the presence of a broken fan (see figure 2 (*b*)) or striated lines on the fan domains. In addition, figure 2 (*c*) shows a mosaic texture of the crystal E phase for compound MD02NA. The transition temperatures plots of series MD*n*2NA versus n, the number of oxyethylene spacer chain, are presented in figure 1 (*a*). As observed in this figure, the presence of these oxyethylene unit chains significantly depress the phase transition temperatures. A similar depressing effect of the oxyethylene on the clearing points and crystalline to nematic transition of nematic LCs has been previously noted [15]. This depression has been attributed to the increased flexibility of these C–O bonds. In addition, the clearing point decreased more than the melting point as the oxyethylene unit increased, thereby tending to result in a depressing mesomorphic ranges at long oxyethylene chains. The decreasing temperature range of the S_A phase as an increasing oxyethylene unit resembles the results of our previous work [11]. On the other hand, the narrow temperature ranges of the S_C^* phase of this series are observed in table 2 as a comparison of mesophase ranges with series MD*n*12A [11]. This series contains three phenyl rings of ester core as mesogenic group, oligo(oxyethylene) spacers and a (*S*)-2-methylbutyl chiral tail.

3.1.2. *Series MDn2NB*

This series differed structurally from the MD*n*2NA series. The (*S*)-2-methylbutyl terminal chiral tail of MD*n*2NA was replaced by the (*R*)-1-methylheptyl chiral moiety. At short derivatives (n=0, 1), the more ordered smectic mesomorphism, crystal E, was observed. On the other hand, a blue phase–cholesteric–twist grain boundary A–smectic A–chiral smectic C (BP–Ch–TGB_A–S_A–S_C^*) phase sequence is presented at long derivatives (n= 1, 2, 3). Figure 3 (*a*) shows the grazed platelet texture of the blue phase for compound MD32NB. Upon cooling

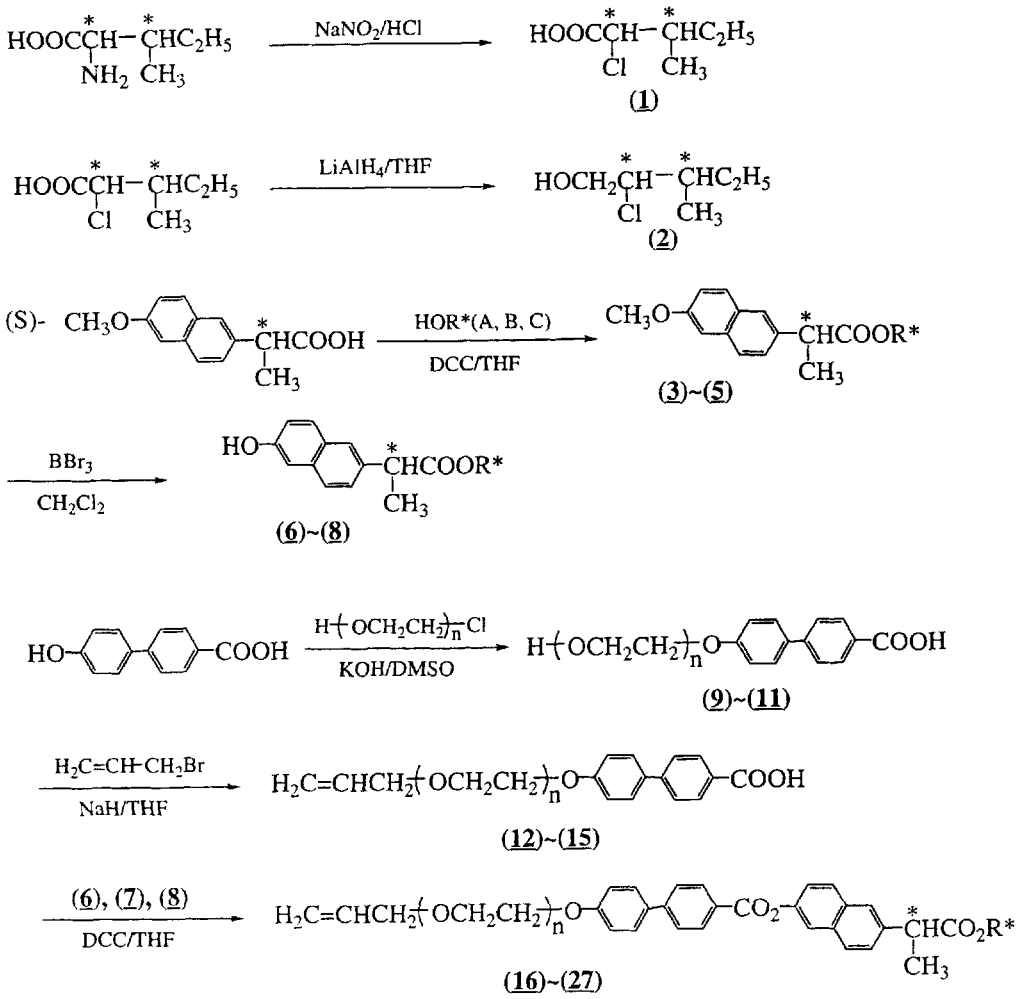

where n= 0, 1, 2, 3

R*=			
A =	$-CH_2\overset{*}{C}HC_2H_5$ (CH3)	(16)~(19)	MDn2NA Series
B =	$-\overset{*}{C}HC_6H_{13}$ (CH3)	(20)~(23)	MDn21B Series
C =	$-CH_2\overset{*}{C}H\overset{*}{C}HC_2H_5$ (Cl, CH3)	(24)~(27)	MDn21C Series

Scheme. The synthesis of ferroelectric liquid crystal MD*n*2NA, MD*n*2NB, and MD*n*2NC series.

from the BP, a Grandjean texture with oily streaks grew gradually during the formation of the cholesteric phase (see figure 3(*b*)). After further cooling from the Grandjean oily streak cholesteric phase, the TGB_A phase appeared as evidenced by the formation of a filament texture (see figure 3(*c*)) [16–18] or an iridescent Grandjean texture [9]. The texture was confirmed by the observation of pitch bands which are perpendicular to the long axes of the filaments. Below the TGB_A phase, the presence of a smectic A phase was observed. The ferroelectric S_C^* phase formed on cooling from the smectic A phase showed the striated lines on the fan domains or a broken fan texture.

The transition temperature is plotted in figure 1(*b*) as

Table 1. Transition temperatures for the series MD*n*2NA, MD*n*2NB, and MD*n*2NC[f].

Name	*n*	Phase transition °C (corresponding enthalpy changes/mJ mg^{-1}) Heating / Cooling
MD02NA	0	Cr 105(−) CrE 113·2(45·7) S_A 168·3(8·5) I / I 166·8(7·3) S_A 98·6(11) CrE 83·8(31·7) Cr
MD12NA	1	Cr 98·6(1·2) CrE 120·1(48·5) S_A 126·3(3·6) I / I 124·8(6·2) S_A 81·3(−) S_C^* 77·1(46·1)[a] Cr
MD22NA	2	Cr 90·6(−) S_A 93·2(77·3)[b] I / I 91·7(4·9) S_A 84·7(1·1) S_C^* 68·6(62·2) Cr
MD32NA	3	Cr 74·11(36·8) I / I 63·5(4·5) S_A 60·0(−) S_C^* 53·4(24·7)[a] Cr
MD02NB	0	Cr 26·2(3·8) S_X 76·3(4·8) CrE 97·6(37·4) S_A 167·3(7·7) I / I 165·9(6·1) S_A 93·7(11·6) CrE 74·5(26·4) S_X 23·2(4·5) Cr
MD12NB	1	Cr 80·9(64·1) S_A 136·2(−) TGB_A 136·3(−) Ch 137·9(2·0)[c] BP 141·1(0·4) I / I 139·6(0·8) BP 136·3(−) Ch 136(−) TGB_A 135·9(2·3)[c] S_A 70·8(11·1) CrE 36·1(2·6) Cr
MD22NB	2	Cr 65·3(31·4) S_A 97·5(−) TGB_A 97·7(−) Ch 102·2(0·8)[c] BP 103·4(0·5) I / I 102·4(0·4) BP 101(−) Ch 97·4(−) TGB_A 97(1·0)[c] S_A 59·2(−)[d] S_C^* 25·1(11·2) Cr
MD32NB	3	Cr 20·5(15·2) S_X 39(18·7) S_C^* 52(−)[d] S_A 70(−) TGB_A 72·6(−) Ch 74·2(0·4)[c] BP 79·6(0·5) I / I 78(0·6) BP 74(−) Ch 72·4(−) TGB_A 69·8(0·6)[c] S_A 50(−)[d] S_C^* 6·2(17·2) Cr
MD02NC	0	Cr 120·0(54·1) S_A 164·2(11·0) I / I 163·1(11·1) S_A 101·4(52·5) Cr
MD12NC	1	Cr 106·4(71·8) S_A 127·3(7·8) I / I 125·8(7·8) S_A 83·8(0·1) S_C^* 72·7(54·9) Cr
MD22NC	2	Cr 92·0(−) S_A 94·5(72·8)[b] I / I 90·9(5·0) S_A 79·7(0·7) S_C^* 66·8(55·5) Cr
MD32NC	3	Cr 57·2(22·9) S_A 63·3(18·1) I / I 58·9(−) S_A 57·4(5·8)[e] S_C^* 43·8(38·8) Cr

[a] $\Delta\bar{H}(S_A–S_C^*–Cr)$.
[b] $\Delta\bar{H}(Cr–S_A–I)$.
[c] $\Delta\bar{H}(S_A–TGB_A–Ch)$.
[d] Enthalpies were too small to be evaluated.
[e] $\Delta\bar{H}(I–S_A–S_C^*)$.
[f] I = isotropic; CrE = crystal E; S_C^* = chiral smectic C; S_A = smectic A; TGB_A = twist grain boundary A; Ch = cholesteric; BP = blue phase; Cr = crystalline phase.

a function of units of the oxyethylene chain. The BP, TGB_A and S_C^* phase ranges increase as the unit of oxyethylene chain increases. However, the Ch and S_A phases show an opposite trend.

A comparison is made in table 3 of the results of the mesomorphic ranges of series MD*n*2NB with series MD*n*12B (n=0, 1, 2, 3). The compounds of series MD*n*12B with a rather narrow S_C^* temperature range have been previously reported [11]. The more rigid mesogen (four phenyl rings of ester core) coupled with the flexible (*R*)-1-methylheptyl of the series MD*n*2NB results in some mesomorphic phenomena as follows: (i) The ΔS_A seems to be affected only slightly. (ii) The ΔS_C^*, ΔTGB_A, ΔCh and ΔBP are present and widen in the series MD*n*2NB. These results could be accounted for by the fact that the more flexible chiral tail is coupled with a more rigid (four phenyl rings of ester core) mesogenic group. Notably, the structural modification of the mesogenic group of the MD*n*2NB series in a oxyethylene spacer/methyheptyl chiral tail system for widening the S_C^* phase was achieved.

3.1.3. *Series MDn2NC*

The last series of compounds, MD*n*2NC, was covalently incorporated with the (2*S*, 3*S*)-2-chloro-3-methylpentyl chiral moiety instead of the (*S*)-2-methylbutyl and (*R*)-1-methylheptyl of MD*n*2NB series and MD*n*2NC series respectively. This type of moiety with two chiral

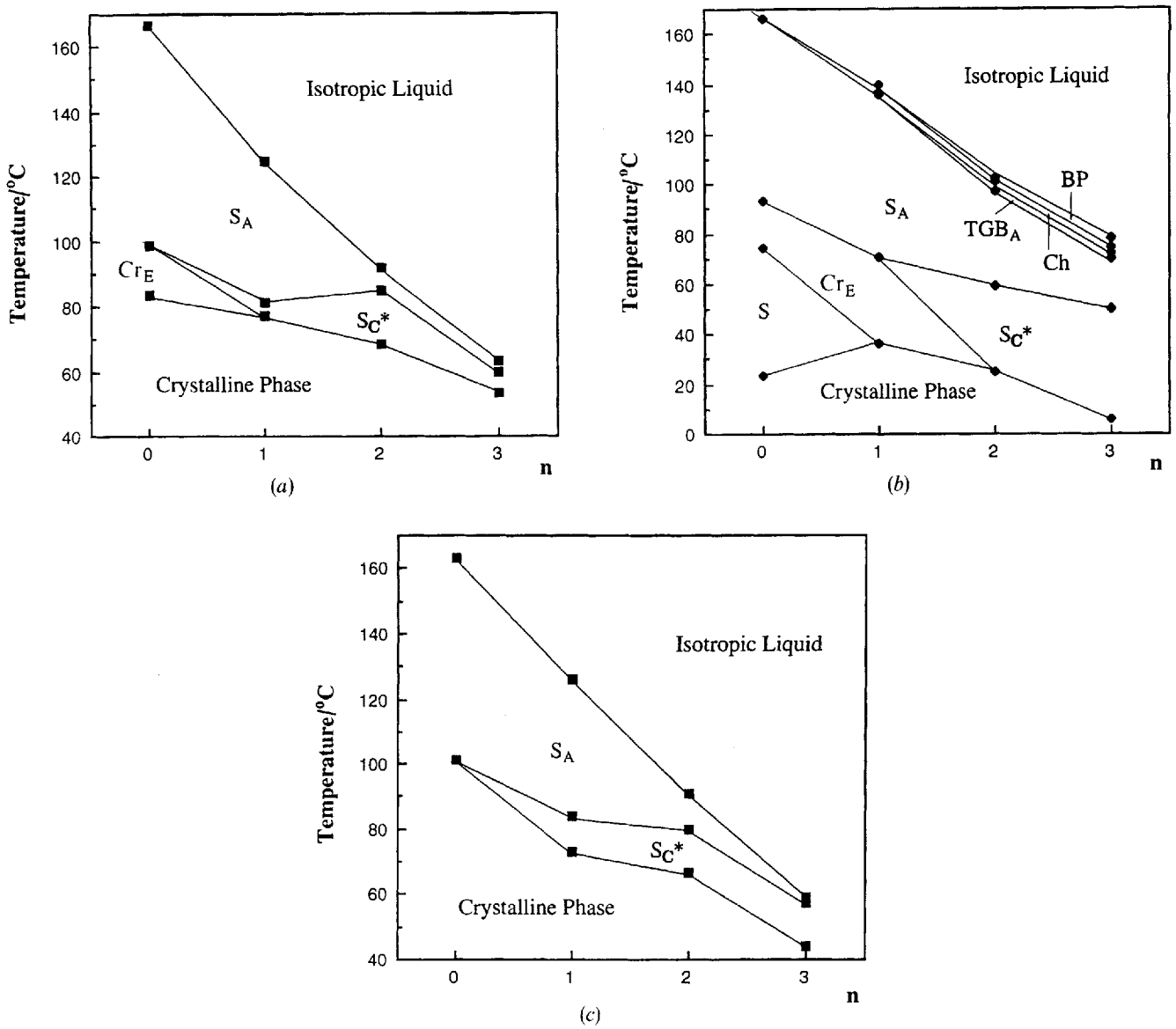

Figure 1. Plots of transition temperatures versus n, the number of oxyethylene spacer chain: (*a*) MDn2NA; (*b*) MDn2NB; (*c*) MDn2NC.

centres has been reported to possess a large spontaneous polarization [9]. The four compounds of this series are all mesomorphic. Different chiral moieties usually result in different mesophase sequences (see figure 1 (*c*)). All of the compounds in this series exhibit similar liquid crystal behaviour: an enantiotropic S_A and a monotropic S_C^*, except the shortest derivative ($n=0$) only reveals an enantiotropic S_A phase. The optical polarizing microscopy results of the S_A and S_C^* phases are the same as the results of series MDn2NA, a focal-conic fan texture for the S_A and a broken fan texture for the S_C^* phases.

Results in figure 1 (*a*), (*b*), and (*c*) indicate that the series MDn2NA and the series MDn2NC have a similar tendency of the formation of liquid crystalline phase. In contrast, the series MDn2NB presents a more different liquid crystalline behaviour due to the more flexible chiral moiety with the more rigid mesogenic group.

3.2. *Calorimetric studies*

Transition enthalpies were determined by differential scanning calorimetry using a Seiko DSC 220C. The transition temperatures and corresponding enthalpies values are listed in table 1. The thermograms were recorded upon cooling at a rate of $10°C\,min^{-1}$ and $5°C\,min^{-1}$ (figure 4 (*a*), (*b*), and (*c*)). For MD12NB,

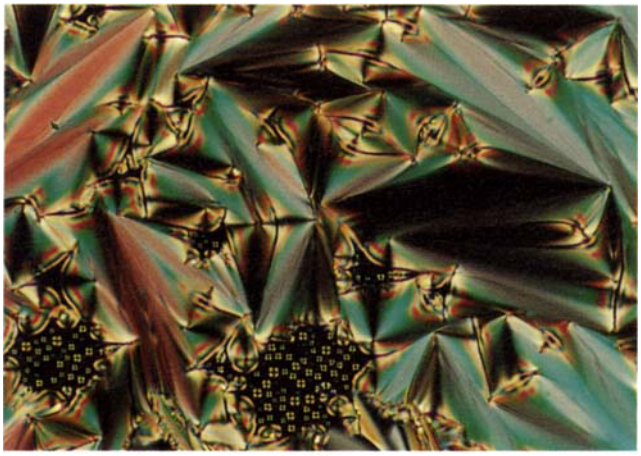

(*a*)

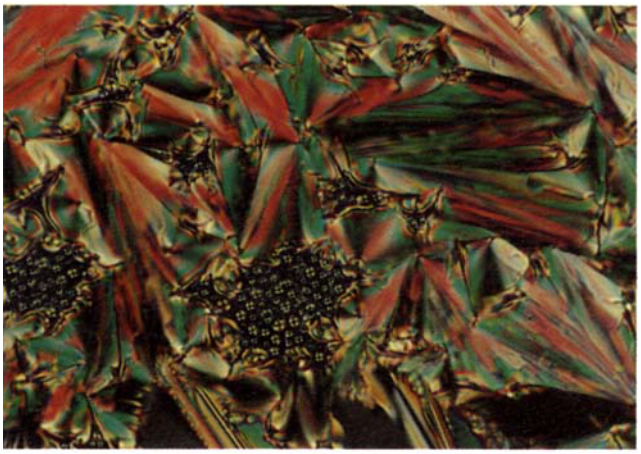

(*b*)

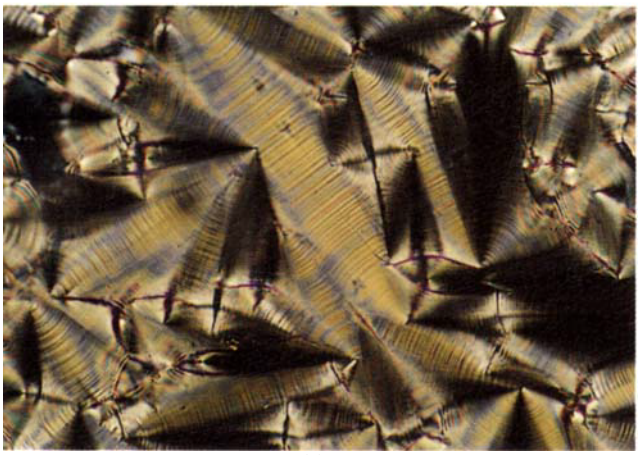

(*c*)

Figure 2. Optical polarizing micrographs: (*a*) the S_A phase of MD22NA at 85°C (400 ×); (*b*) the S_C^* phase of MD22NA at 83·7°C (400 ×); (*c*) the CrE phase of MD02NA at 119·2°C (400 ×).

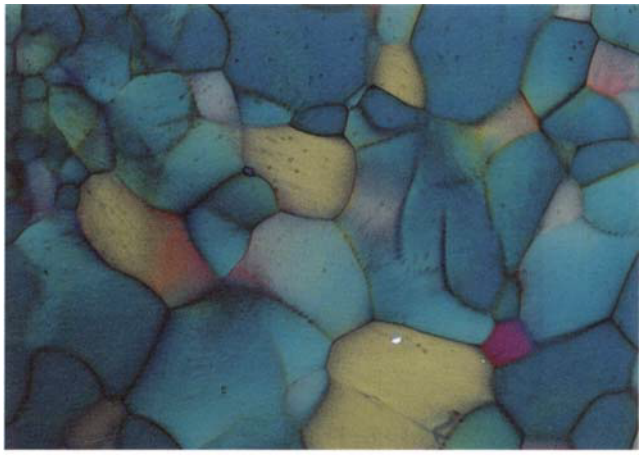

(*a*)

(*b*)

(*c*)

Figure 3. Optical polarizing micrographs of MD32NB: (*a*) the blue phase at 75°C (400 ×); (*b*) the cholesteric phase at 73·6°C (400 ×); (*c*) the TGB_A phase at 71°C (400 ×).

Table 2. Mesophase ranges for the series MDn2NA and MDn12A.

Compound	*n*	Mesogenic core[a]	ΔT_M[b]	ΔS_C^*	ΔS_A	ΔTGB_A§	ΔCh	ΔBP§	Reference
MD02NA	0	M_{2N}	83	–	68·2	–	–	–	[this work]
MD12NA	1	M_{2N}	47·7	4·1	43·5	–	–	–	[this work]
MD22NA	2	M_{2N}	23·1	16·1	7	–	–	–	[this work]
MD32NA	3	M_{2N}	10·1	6·6	3·5	–	–	–	[this work]
MD012A	0	M_{12}	125·6	–	81·5	–	42	2	[11]
MD112A	1	M_{12}	150·4	91·5	32·7	0·9	17·4	7·9	[11]
MD212A	2	M_{12}	116·9	86·5	15·3	1·6	11·1	2·4	[11]
MD312A	3	M_{12}	111·3	91·3	2·2	3·8	5·5	8·5	[11]

[a] M_{2N}= 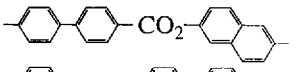

M_{12}= 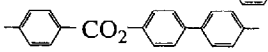

[b] ΔT_M = Total temperature range of mesophase.
§The values were determined by POM.

Table 3. Mesophase ranges for the series MD*n*2NB and MD*n*12B.

Compound	*n*	Mesogenic core[a]	ΔT_M[b]	ΔS_C^*	ΔS_A	ΔTGB_A[d]	ΔCh	ΔBP[d]	Reference
MD02NB	0	M_{2N}	142·7	–	72·2	–	–	–	[this work]
MD12NB	1	M_{2N}	103·5	–	65·1	0·1	0·3	3·3	[this work]
MD22NB	2	M_{2N}	77·3	34·1	37·.8	0·4	3·6	1·4	[this work]
MD32NB	3	M_{2N}	71·8	43·8	19·8	2·6	1·6	4	[this work]
MD012B	0	M_{12}	99·8	–	99·8	–	–	–	[11]
MD112B	1	M_{12}	77·6	3·2	74·4	–	–	–	[11]
MD212B	2	M_{12}	31·7	1·3	30·4	–	–	–	[11]
MD312B	3	M_{12}	66·05	–[c]	4·32	–	–	–	[11]

[a] M_{2N}= 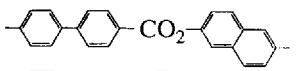

M_{12}= 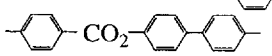

[b] ΔT_M = Total temperature range of the mesophase.
[c] The temperature is too low to investigate.
[d] The values were determined by POM.

MD22*n*B, and MD32NB, obtaining individual transition enthalpies from the BP/Ch and TGB_A/S_A phases due to overlapping was relatively difficult. Only the melting transition enthalpies could be determined unambiguously. The enthalpies of some overlapping phase transitions are summarized in table 1. Some compounds of the three series underwent a larger degree of supercooling (max: 40°C for MD22NB).

3.3. *X-ray investigations*

The presence of the S_C^* phase and the other ordered smectic phases were confirmed by X-ray diffraction measurements. Figures 5(*a*) and (*b*) show representative X-ray diffractograms obtained from powder samples of MD02NB and MD32NB, respectively. A broad reflection at wide angles (associated with the lateral packing) and a sharp reflection at small angles (associated with the smectic layers) are shown in curve A of figure 5(*a*), and by all curves in figure 5(*b*). Curve A in figure 5(*a*) exhibits a rather diffuse reflection at around 4·535 Å, a sharp first-order reflection at 35·9432 Å. These results combined with optical polarizing microscopy observations correlate with the S_A phase. Curve B in figure 5(*a*) presents three sharp reflections at wide angles, 5·323, 4·001, and 3·231 Å, respectively. Moreover, the sharp first order reflection is presented at a small angle, 37·6123 Å. These results correlate sufficiently with the optical polarizing microscopy observation, indicating a crystal E phase [20]. On the other hand, the S_C^* phase showed a decreased layer spacing from 36·1937 Å to 34·0401 Å as the temperature cooled from the S_A phase, as presented in figure 5(*b*). This is important evidence of the formation of molecular tilt in the ferroelectric S_C^* phase.

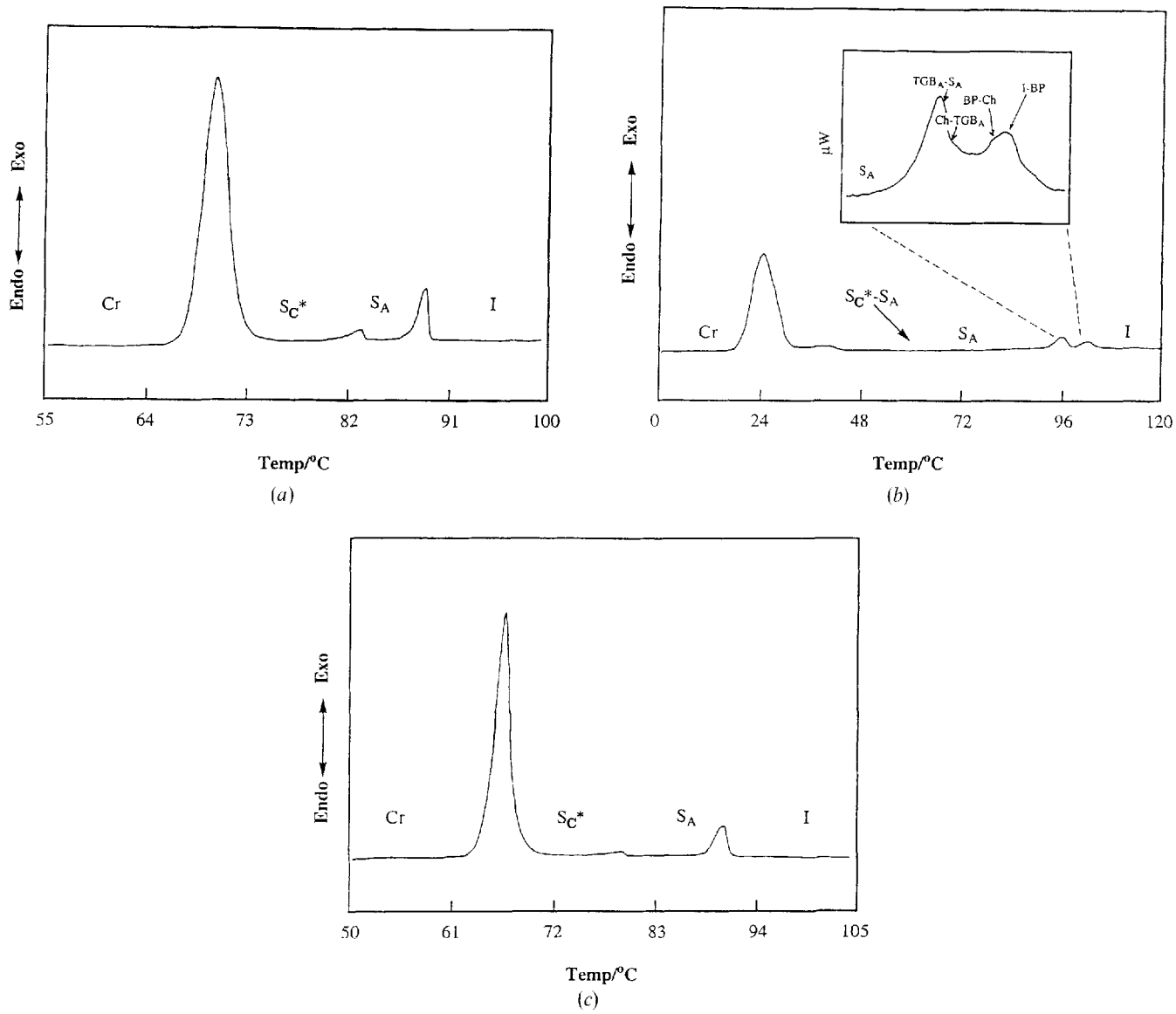

Figure 4. DSC thermograms of (*a*) MD22NA (5°C min^{-1}, cooling scan), (*b*) MD22NB (5°C min^{-1}, cooling scan), (*c*) MD22NC (5°C min^{-1}, cooling scan).

4. Conclusions

The novel ferroelectric liquid crystals containing a (2*S*)-2-(6-(4-hydroxybiphenyl-4′-carbonyloxy)-2′-naphthyl)propionate mesogenic group, oligo(oxyethylene) spacer and three different chiral moieties, (*S*)-2-methylbutyl, (*R*)-1-methylheptyl, and (2*S*, 3*S*)-2-chloro-3-methylpentyl were synthesized. All the compounds were liquid crystalline. The oxyethylene unit as the spacer chain favoured a lowering of the transition temperatures. Results in this study above indicated that the MD*n*2NB series exhibit a more rich mesomorphism, BP, Ch, TGB_A, S_A, S_C^*, CrE, than the other two series, MD*n*2NA and MD*n*2NC. Moreover, the S_C^* phase ranges of series MD*n*2NB are larger than the other two series. Series MD*n*2NA, and MD*n*2NC have a similar mesomorphic sequence, S_A, S_C^*, and CrE. These results imply that the more flexible (*R*)-1-methylheptyl chiral tail and four phenyl rings of the ester mesogenic core (–Ph–Ph COO–naph–) tend to give rise to a higher thermal stability of the mesophases, especially in the chiral smectic C phase.

5. Experimental

5.1. *Materials*

(*S*)-2-(6-Methoxy-2-naphthyl)propionic acid, 4′-hydroxy-4-biphenylcarboxylic acid, (*R*)-2-octanol (from

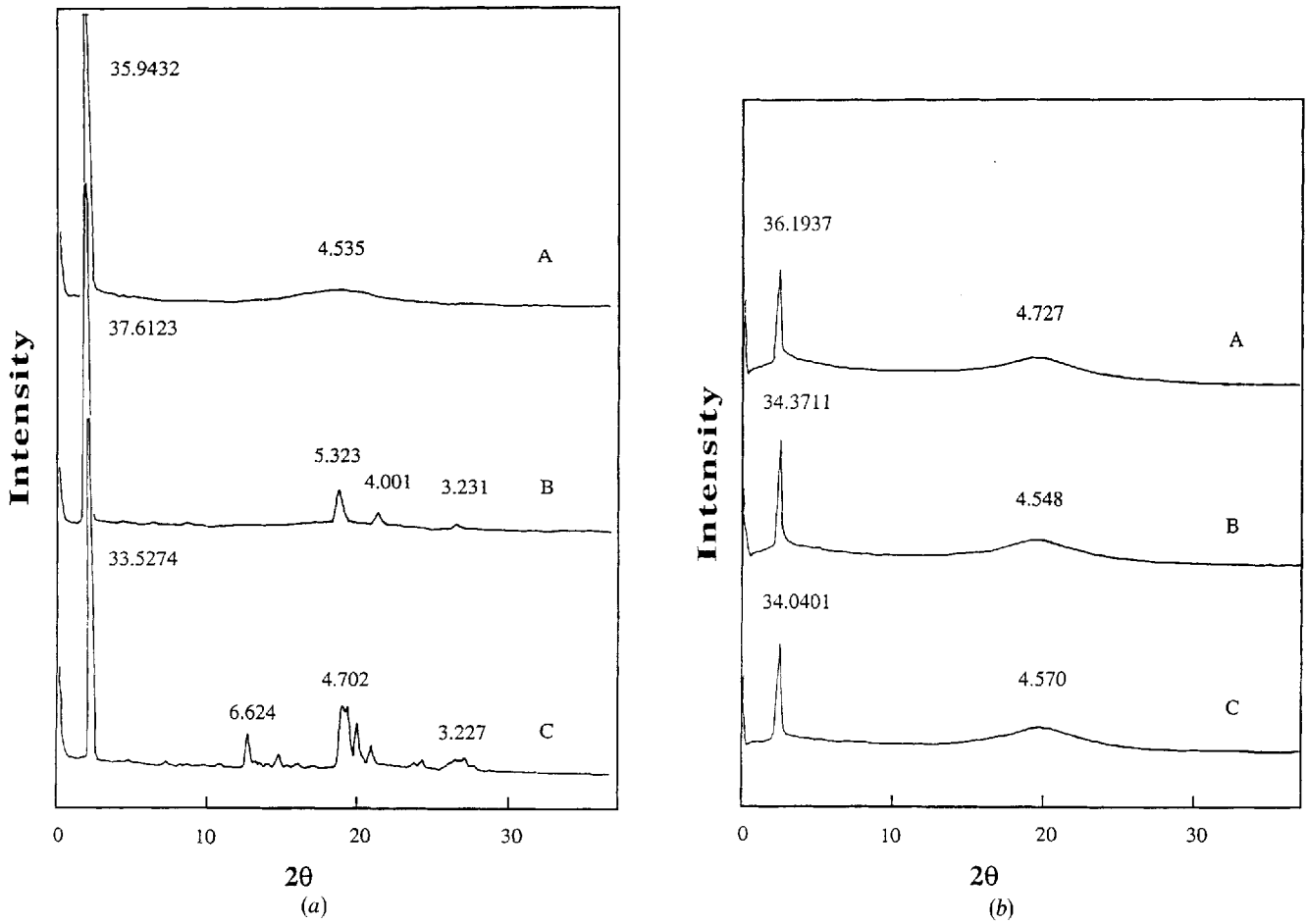

Figure 5. (*a*) Temperature dependence of powder X-ray diffraction measurements for MD02NB at (A) 108, (B) 93, (C) 25°C; (*b*) temperature dependence of the powder X-ray diffraction measurements for MD32NB at (A) 61, (B) 48, (C) 43°C.

TCI); allyl bromide, 2-chloroethanol, 2-(2-chloroethoxy) ethanol, 2-(2-(2-chloroethoxy)ethoxy)ethanol (from Aldrich); (*S*)-2-methyl-butan-1-ol (from Fluka); and boron tribromide and other reagents (from Merck) were used directly for the synthesis.

5.2. *Measurements*

^{1}H NMR spectra were obtained with a Bruker AM300 MHz spectrometer. All spectra were recorded in $CDCl_3$ with TMS as the internal standard unless otherwise noted. A Seiko DSC 220C differential scanning calorimeter equipped with a 5200H computer system was used to determine the thermal transitions that were read at the maximum of their endothermic or exothermic peaks. In all cases, heating and cooling rates were 5°C min^{-1}, unless otherwise specified. After the first heating scan, the sample was annealed at 10°C above the isotropization temperature for 5–10 min. Under these conditions, beginning with the second heating and cooling scans, all recorded DSC scans gave reproducible data. The transitions reported were read during the second or third heating scans and cooling scans unless otherwise specified. A Nikon Microphot-FX optical polarized microscope equipped with a Mettler FP 82 hot stage and a Mettler FP 80 central processor was used in observing thermal transitions and anisotropic textures. X-ray diffraction measurements were performed with a Rigaku R-Axis IIC powder diffractometer. Two Imaging Plate (IP) detectors were used so that reflection spot exposure and readout operations could be performed. This feature provides increased data collection efficiency and minimizes the time required for IP residual image erasure. The monochromatized X-ray beam from nickel-filtered CuK_α radiation with a wavelength of 0·15406 nm was used. A temperature controller was added to the X-ray apparatus for thermal measurements. The precision of the controller was ±0·5°C in the temperature range studied.

5.3. *Synthesis*

5.3.1. *(2S, 3S)-2-Chloro-3-methyl pentanoic acid* (**1**)

The synthesis of compound (**1**) is according to the method of Koppenhoefer [21]. In a 500 ml, round-bottomed flask equipped with a magnetic stirrer were placed L-isoleucine (0·2 mol) and 360 ml 5 M HCl at 0°C. The cooled sodium nitrite aqueous solution (0·3 mol) was added dropwise under nitrogen below 4°C. After stirring the reaction mixture for 5 h, the ice bath was removed and the mixture stirred at RT for 24 h. 16 g of calcium carbonate was added, and extracted with ethyl ether. The organic phase was washed with a 10 wt % aqueous solution of HCl, and the solvent was evaporated on a rotavapor. The colourless oily product was obtained by vacuum distillation (110°C/8 mmHg, Yield 84·7 per cent). $[\alpha]_D^{25} = 7{\cdot}6$, ^{1}H NMR ($CDCl_3$, TMS): $\delta = 0{\cdot}9$ (t, 3 H, $-CH_2\underline{CH_3}$), 0·97 (d, 3 H, $-CH(\underline{CH_3})-C_2H_5-$), 1·28 and 1·60 (m, 2 H, $-\underline{CH_2}CH_3$), 2·07 (m, 1 H, $-\underline{CH}CH_3-$), 4·25 (m, 1 H, $-\underline{CH}Cl-COOH$).

5.3.2. *(2S, 3S)-2-Chloro-3-methylpentanol* (**2**)

A solution of compound (**1**), 5 g in dry THF (30 ml), was added dropwise to a stirred, cooled (−70°C) mixture of $LiAlH_4$ (2·8 g) and dry THF (30 ml) under a nitrogen atmosphere. The stirred mixture was allowed to warm to room temperature and then heated under reflux for 2 h. Excess $LiAlH_4$ was quenched with ethyl acetate (50 ml), and the mixture was treated with 10 per cent HCl (300 ml). The product was extracted into ethyl acetate twice, and the combined organic layers were dried over anhydrous $MgSO_4$. The solvent was evaporated off, and the remaining crude product was purified by column chromatography (silica gel; hexane–ethyl acetate 10:1) to give a colourless liquid (yield 40 per cent). ^{1}H NMR ($CDCl_3$, TMS): δ(ppm) = 0·9 (t, 3 H, $\underline{CH_3}CH_2-$), 0·93 (d, 3 H, $-CH(\underline{CH_3})-$), 1·09–1·37, 1·47–1·90 (m, 3 H, $CH_3\underline{CH_2}\underline{CH}(CH_3)-$), 2·48 (s, 1 H, $-\underline{OH}$), 3·61–3·85 (m, 2 H, $-\underline{CH_2}OH$), 4·15–4·53 (m, 1 H, $-\underline{CH}(Cl)-$).

5.3.3. *(S)-2-Methylbutyl (2S)-2-(6-methoxy-2-naphthyl)propionate* (**3**), *(R)-1-methylheptyl (2S)-2-(6-methoxy-2-naphthyl)propionate* (**4**) *and (2S, 3S)-2-chloro-3-methylpentyl (2S)-2-(6-methoxy-2-naphthyl)propionate* (**5**)

These compounds were synthesized by a similar method; for example, compound (**3**): In a 250 ml round flask, (*S*)-2-(6-methoxy-2-naphthyl)propionic acid (5 g, 0·022 mol), (*S*)-2-methyl-butan-1-ol (3·03 ml, 0·028 mol), DCC (dicyclohexylcarbodiimide) (4·532 g, 0·022 mol), DMAP (4-(dimethylamino)pyridine) (0·045 g, 0·0004 mol) and dried tetrahydrofuran (100 ml) were stirred under nitrogen at 4°C overnight. The solution was filtered and the filtrate was washed with 10 per cent HCl and 5 per cent $NaHCO_3$. The filtrate was then evaporated to a crudely yellow solid. The product was purified by flash chromatography on silica gel with 25 per cent ethyl acetate in hexane to yield 6·389 g (88 per cent). m.p.: (**3**), (**4**), (**5**) < 25°C. ^{1}H NMR ($CDCl_3$, TMS): δ (ppm) = (**3**) 0·88 (m, 6 H, $-CH(\underline{CH_3})-CH_2\underline{CH_3}$), 1·10–1·34 (m, 2 H, $-\underline{CH_2}CH_3$), 1·57 (d, 3 H, $-CH(\underline{CH_3})-COO-$), 1·8 (m, 1 H, $-\underline{CH_2}\underline{CH}(CH_3)-$), 3·8–3·9 (q, 1 H, $-\underline{CH}(CH_3)-COO-$), 3·9 (s, 3 H, $\underline{CH_3}O-$), 4·2 and 4·3 (m, 2 H, $-O-\underline{CH_2}-$), 7·1–7·7 (m, 6 H, aromatic protons). (**4**) 0·85 (t, 3 H, $-(CH_2)_5\underline{CH_3}$), 1·05–1·45 (m, 13 H, $-(\underline{CH_2})_5CH_3$, $-OCH(\underline{CH_3})-$), 1·59 (d, 3 H, $-CH(\underline{CH_3})-COO-$), 3·7–3·95 (m, 3 H, $-\underline{CH}(CH_3)-COO-$, $-OCH_2(\underline{CH_3})-$), 3·9 (s, 3 H, $\underline{CH_3}O-$), 7·1–7·7 (m, 6 H, aromatic protons). (**5**) 0·78–0·88 (m, 6 H, $-CH(\underline{CH_3})CH_2\underline{CH_3}$), 1·0–1·2 (m, 2 H, $-\underline{CH_2}CH_3$), 1·35–1·45 (m, 1 H, $-\underline{CH}(CH_3)CH_2-$), 1·58 (d, 3 H, $-CH(\underline{CH_3})-COO-$), 3·79–4·32 (m, 4 H, $-\underline{CH}(CH_3)-COO-$, $-OCH_2\underline{CH}(Cl)-$), 3·9 (s, 3 H, $\underline{CH_3}O-$), 7·09–7·58 (m, 6 H, aromatic protons).

5.3.4. *(S)-2-Methyl-1-butyl (2S)-2-(6-hydroxy-2-naphthyl)propionate* (**6**), *(R)-1-methylheptyl (2S)-2-(6-hydroxy-2-naphthyl)propionate* (**7**) *and (2S, 3S)-2-chloro-3-methylpentyl (2S)-2-(6-hydroxy-2-naphthyl) propionate* (**8**)

The ester (**3**) (5 g, 0·015 mol) dissolved in dried dichloromethane (56 ml) had BBr_3 (boron tribromide) (2·778 ml (0·029 mol) added at −20°C. The mixture was stirred at −20°C for 5 min, and 0°C for 50 min. After diluting with dichloromethane (112 ml), the solution was poured into a mixture of saturated ammonium chloride 56 ml and ice (56 g). The organic layer was separated and washed with brine–ice, dried over anhydrous magnesium sulphate, and concentrated *in vacuo*. The residue was purified by column chromatography over silica gel using dichloromethane as eluent. The product (**6**) (80·3 per cent yield) was collected after recrystallization from hexane. (**6**) ^{1}H NMR ($CDCl_3$, TMS): δ (ppm) = 0·8 (m, 6 H, $-CH(\underline{CH_3})-CH_2\underline{CH_3}$), 1·3 and 1·5 (m, 2 H, $-\underline{CH_2}CH_3$), 1·6 (d, 3 H, $-\underline{CH}(\underline{CH_3})-COO-$), 1·8 (m, 1 H, $-\underline{CH_2}\underline{CH}(CH_3)-$), 3·8–3·9 (q, 1 H, $-\underline{CH}(CH_3)-COO-$), 4·2 and 4·3 (m, 2 H, $-O-\underline{CH_2}-$), 7·1–7·7 (m, 6 H, aromatic protons). (**7**) ^{1}H NMR ($CDCl_3$, TMS): δ (ppm) = 0·8 (t, 3 H, $-(CH_2)_5\underline{CH_3}$), 1·08–1·48 (m, 13 H, $-(\underline{CH_2})_5CH_3$, $-OCH(\underline{CH_3})-$), 1·06 (d, 3 H, $-CH(\underline{CH_3})-COO-$), 3·8–3·95 (m, 2 H, $-\underline{CH}(CH_3)-COO-$, $-\underline{OCH}(CH_3)\underline{CH_2}-$), 7·0–7·65 (m, 6 H, atomatic protons). (**8**) ^{1}H NMR ($CDCl_3$, TMS): δ (ppm) = 0·85–0·94 (m, 6 H, $-CH(\underline{CH_3})CH_2\underline{CH_3}$), 1·02–1·28 (m, 2 H, $-CH(\underline{CH_3})\underline{CH_2}CH_3$), 1·3–1·4 (m, 1 H, $-\underline{CH}(CH_3)CH_2-$, 1·52 (d, 3 H, $-CH(\underline{CH_3})-COO-$), 3·79–4·32 (m, 4 H, $-\underline{CH}(CH_3)-COO-$, $-\underline{OCH_2}\underline{CH}(Cl)-$), 7·25–7·7 (m, 6 H, aromatic protons).

5.3.5. *4'-(2-Hydroxyethoxy)-4-biphenylcarboxylic acid* (**9**), *4'-(2-(2-hydroxyethoxy)ethoxy)-4-biphenylcarboxylic acid* (**10**) *and 4'-(2-(2-(2-hydroxyethoxy)ethoxy)ethoxy)-4-biphenylcarboxylic acid* (**11**)

These compounds were synthesized by the same method. As an example, the synthesis of 4'-(2-(2-hydroxyethoxy)ethoxy)-4-biphenylcarboxylic acid (**10**) is presented as follows: A solution of 2-(2-chloroethoxy)ethanol (3·198 g, 0·026 mol) in 5 ml of DMSO (dimthylsulphoxide) was added dropwise to a solution of 4'-hydroxy-4-biphenylcarboxylic acid (2·5 g, 0·012 mol) and powdered potassium hydroxide (2·088 g, 0·037 mol) in 15 ml of DMSO at 70°C. After stirring the reaction mixture under reflux for 24 h, the solution was poured into 300 ml water. The mixture solution was acidified with hydrochloric acid. After cooling to 0°C, a white solid was filtered and set aside. The filtrate was extracted with tetrahydrofuran and the extracted material was evaporated to a white solid which was combined with the set-aside material. The combined material (75 per cent yield) was recrystallized from hexane. m.p. 213°C. ^{1}H NMR ($CDCl_3$, TMS): (δ (ppm) = 2·62 (s, 1, –OH), 3·81–4·25 (m, 8 H, –(OCH_2CH_2)$_2$–), 6·9, 7·5, 7·6 and 8·1 (4d, 8 H, aromatic protons), 12·2 (s, 1 H, –COOH).

5.3.6. *4'-Allyloxy-4-biphenylcarboxylic acid* (**12**), *4'-(2-allyloxyethoxy)-4-biphenylcarboxylic acid* (**13**), *4'-(2-(2-allyloxyethoxy)ethoxy)-4-biphenylcarboxylic acid* (**14**), *and 4'-(2-(2-(2-allyloxyethoxy)ethoxy)ethoxy)-4-biphenylcarboxylic acid* (**15**)

These compounds were synthesized by a similar method. As an example, the synthesis of 4'-(2-(2-allyloxyethoxy)ethoxy)-4-biphenylcarboxylic acid (**14**) is presented as follows: The 4'-(2-(2-hydroxyethoxy)ethoxy)-4-biphenylcarboxylic acid (**10**) (3 g, 0·01 mol) was added to a suspension of (1·91 g, 0·079 mol) sodium hydride in 50 ml dried tetrahydrofuran at 4°C. After the hydrogen was completely released, allyl bromide (3 ml, 0·034 mol) was added dropwise to

Table 4. ^{1}H NMR data of the MD*n*2NA series.

Monomer	^{1}H NMR ($CDCl_3$, δ ppm)
MD02NA	0·80–0·90 (m, 6 H, –CHCH_3–CH_2–CH_3), 1·10–1·40 (m, 2 H, –CH_2–CH_3), 1·55–1·70 (m, 4 H, –CH_2–CHCH_3–, –CHCH_3–COO–), 3·90–4·05 (m, 3 H, –CHCH_3–COO–, –O–CH_2–$CHCH_3$–), 4·66 (d, 2 H, =CH–CH_2–O–), 5·45 (m, 2 H, CH_2=CH–), 6·12 (m, 1 H, CH_2=CH–), 7·05–8·32 (m, 14 H, aromatic proton)
MD12NA	0·75–0·85 (m, 6 H, –CHCH_3–CH_2–CH_3), 1·05–1·38 (m, 2 H, –CH_2–CH_3), 1·5–1·65 (m, 4 H, –CH_2–CHCH_3–, –CHCH_3–COO–), 3·79–4·19 (m, 9 H, –CHCH_3–COO–, –O–CH_2–$CHCH_3$–, –O–CH_2–CH_2–O–, =CH–CH_2–O–), 5·24 (m, 2 H, CH_2=CH–), 5·92 (m, 1 H, CH_2=CH–), 7·0–8·25 (m, 14 H, aromatic proton)
MD22NA	0·79–0·89 (m, 6 H, –CHCH_3–CH_2–CH_3), 1·05–1·40 (m, 2 H, –CH_2–CH_3), 1·50–1·65 (m, 4 H, –CH_2–CHCH_3–, –CHCH_3–COO–), 3·60–4·25 (m, 13 H, –CHCH_3–COO–, –O–CH_2–$CHCH_3$–, –O–(CH_2–CH_2)$_2$–O–, =CH–CH_2–O–), 5·25 (m, 2 H, CH_2=CH–), 5·92 (m, 1 H, CH_2=CH–), 7·0–8·30 (m, 14 H, aromatic proton)
MD32NA	0·80–0·90 (m, 6 H, –CHCH_3–CH_2–CH_3), 1·05–1·38 (m, 2 H, –CH_2–CH_3), 1·50–1·70 (m, 4 H, –CH_2–CHCH_3–, –CHCH_3–COO–), 3·40–4·25 (m, 17 H, –CHCH_3–COO–, –O–CH_2–$CHCH_3$–, –O–(CH_2–CH_2)$_3$–O–, =CH–CH_2–O–), 5·19 (m, 2 H, CH_2=CH–), 5·85 (m, 1 H, CH_2=CH–), 7·0–8·25 (m, 14 H, aromatic proton)

Table 5. ^{1}H NMR data of the MD*n*2NB series.

Monomer	^{1}H NMR ($CDCl_3$, δ ppm)
MD02NB	0·85 (t, 3 H, –(CH_2)$_5$–CH_3), 1·05–1·45 (m, 13 H, –(CH_2)$_5$–CH_3, –O–CHCH_3–CH_2–), 1·5 (d, 3 H, –CHCH_3–COO–), 3·8–3·9 (q, 1 H, –CHCH_3–COO–), 4·85–4·92 (m, 1 H, –O–CHCH_3–), 5·28–5·45 (m, 2 H, CH_2=CH–), 6·0–6·12 (m, 1 H, CH_2=CH–), 7·05–8·32 (m, 14 H, aromatic proton)
MD12NB	0·8 (t, 3 H, –(CH_2)$_5$–CH_3), 1·08–1·48 (m, 13 H, –(CH_2)$_5$–CH_3), –O–CHCH_3–CH_2–), 1·59 (d, 3 H, –CH–CH_3–COO–), 3·80–4·20 (m, 7 H, –CHCH_3–COO–, —CH_2–(O–CH_2–CH_2)–O–), 4·88–4·93 (m, 1 H, –O–CHCH_3–), 5·20–5·35 (m, 2 H, CH_2=CH–), 5·90–6·01 (m, 1 H CH_2=CH–), 7·0–8·25 (m, 14 H, aromatic proton)
MD22NB	0·85 (t, 3 H, –(CH_2)$_5$–CH_3), 1·05–1·49 (m, 13 H, –(CH_2)$_5$–CH_3), –O–CHCH_3–CH_2–), 1·6 (d, 3 H, –CHCH_3–COO–), 3·60–4·20 (m, 11 H, –CHCH_3–COO–, –CH_2–(O–CH_2–CH_2)$_2$–O–), 4·85–4·90 (m, 1 H, –O–CHCH_3–), 5·15–5·27 (m, 2 H, CH_2=CH–), 5·88–5·98 (m, 1 H, CH_2=CH–), 7·0–8·25 (m, 14 H, aromatic proton)
MD32NB	0·88 (t, 3 H, –CH_2)$_5$–CH_3), 1·06–1·48 (m, 13 H, –(CH_2)$_5$–CH_3), –O–CHCH_3–CH_2–), 1·58 (d, 3 H, –CHCH_3–COO–), 3·60–4·20 (m, 15 H, –CHCH_3–COO–, –CH_2–(–O–CH_2–CH_2)$_3$–O–), 4·88–4·92 (m, 1 H, –O–CHCH_3–), 5·15–5·29 (m, 2 H, CH_2=CH–), 5·85–5·95 (m, 1 H, CH_2=CH–), 7·0–8·25 (m, 14 H, aromatic proton)

Table 6. ^{1}H NMR data of the MD*n*2NC series.

Monomer	^{1}H NMR ($CDCl_3$, δ ppm)
MD02NC	0·75–0·90 (m, 6 H, $-CHCH_3-CH_2-CH_3$), 1·08–1·29 (m, 2 H, $-CH_2-CH_3$), 1·3–1·41 (m, 1 H, $-CHCl-CHCH_3-$), 1·59 (d, 3 H, $-CHCH_3-COO-$), 3·85–4·35 (m, 4 H, $-CHCH_3-COO-$, $-O-CH_2-CHCl-$), 4·59 (d, 2 H, $=CH-CH_2-O-$), 5·44 (m, 2 H, $CH_2=CH-$), 6·0 (m, 1 H, $CH_2=CH-$), 7·0–8·25 (m, 14 H, aromatic proton)
MD12NC	0·75–0·92 (m, 6 H, $-CHCH_3-CH_2-CH_3$), 1·05–1·27 (m, 2 H, $-CH_2-CH_3$), 1·29–1·41 (m, 1 H, $-CHCl-CHCH_3-$), 1·58 (d, 3 H, $-CHCH_3-COO-$), 3·80–4·35 (m, 10 H, $-CHCH_3-COO-$, $-O-CH_2-CHCl-$, $-O-CH_2-CH_2-O-$, $=CH-CH_2-O-$), 5·26 (m, 2 H, $CH_2=CH-$), 5·85 (m, 1 H, $CH_2=CH-$), 7·01–8·26 (m, 14 H, aromatic proton)
MD22NC	0·75–0·95 (m, 6 H, $-CHCH_3-CH_2-CH_3$), 1·05–1·29 (m, 2 H, $-CH_2-CH_3$), 1·31–1·4 (m, 1 H, $-CHCl-CHCH_3-$), 1·58 (d, 3 H, $-CHCH_3-COO-$), 3·62–4·3 (m, 14 H, $CHCH_3-COO-$, $-O-CH_2-CHCl-$, $-(O-CH_2-CH_2)_2-O-$, $=CH-CH_2-O-$), 5·22 (m, 2 H, $CH_2=CH-$), 5·9 (m, 1 H, $CH_2=CH-$), 7·01–8·26 (m, 14 H, aromatic proton)
MD32NC	0·75–0·95 (m, 6 H, $-CHCH_3-CH_2-CH_3$), 1·04–1·3 (m, 2 H, $-CH_2-CH_3$), 1·31–1·42 (m, 1 H, $-CHCl-CHCH_3-$), 1·6 (d, 3 H, $-CHCH_3-COO-$), 3·65–4·35 (m, 18 H, $-CHCH_3-COO-$, $-O-CH_2-CHCl-$, $-(O-CH_2-CH_2)_3-O-$, $=CH-CH_2-O-$), 5·23 (m, 2 H, $CH_2=CH-$), 5·91 (m, 1 H, $CH_2=CH-$), 7·01–8·27 (m, 14 H, aromatic proton)

the reaction mixture and then stirred at room temperature overnight. The excess sodium hydride was treated with distilled water and extracted with ethyl acetate. The organic phase was washed with 10 per cent aqueous hydrochloric acid solution, dried over anhydrous magnesium sulphate, and the solvent evaporated on a rotary evaporator. The yellow solid product was purified by recrystallization from hexane (72 per cent yield) m.p. 189·8°C. ^{1}H NMR ($CDCl_3$, TMS): δ (ppm)= 3·81–4·25 (m, 10 H, $-CH_2-(OCH_2CH_2)_2-$), 5·23 and 5·9 (m, 3 H, $CH_2=CH-$), 6·9, 7·5, 7·6 and 8·1 (4d, 8 H, aromatic protons), 12·2 (s, 1 H, $-COOH$).

5.3.7. *MDn2NA series:*

[(S)-2-Methyl-1-butyl (2S)-2-(6-(4′-allyloxy-4-biphenylcarbonyloxy)-2-naphthyl)propionate (**16**), *(S)-2-methyl-1-butyl (2S)-2-(6-(4′-(2-allyloxyethoxy)-4-biphenylcarbonyloxy)-2-naphthyl)propionate* (**17**), *(S)-2-methyl-1-butyl (2S)-2-(6-(4′-(2-(2-allyloxyethoxy)-ethoxy)-4-biphenylcarbonyloxy)-2-naphthyl)propionate* (**18**), *(S)-2-methyl-1-butyl (2S)-2-(6-(4′-(2-(2-(2-allyloxyethoxy)ethoxy)ethoxy)-4-biphenylcarbonyloxy)-2-naphthyl)propionate* (**19**)];

MDn2NB series:

[(R)-1-Methylheptyl (2S)-2-(6-(4′-allyloxy-4-biphenylcarbonyloxy)-2-naphthyl)propionate (**20**), *(R)-1-methylheptyl (2S)-2-(6-(4′-(2-allyloxyethoxy)-4-biphenylcarbonyloxy)-2-naphthyl)propionate* (**21**), *(R)-1-methylheptyl (2S)-2-(6-(4′-(2-(2-allyloxyethoxy)-ethoxy)-4-biphenylcarbonyloxy)-2-naphthyl)propionate* (**22**), *(R)-1-methylheptyl (2S)-2-(6-(4′-(2-(2-(2-allyloxyethoxy)ethoxy)ethoxy)-4-biphenylcarbonyloxy)-2-naphthyl)propionate* (**23**)];

MDn2NC series:

[(2S,3S)-2-Chloro-3-methylpentyl (2S)-2-(6-(4′-allyloxy-4-biphenylcarbonyloxy)-2-naphthyl)propionate (**24**), *(2S, 3S)-2-chloro-3-methylpentyl (2S)-2-(6-(4′-(2-allyloxyethoxy)-4-biphenylcarbonyloxy)-2-naphthyl-propionate* (**25**), *(2S, 3S)-2-chloro-3-methylpentyl (2S)-2-(6-(4′-(2-(2-allyloxyethoxy)ethoxy)-4-biphenylcarbonyloxy)-2-naphthyl)propionate* (**26**), *(2S, 3S)-2-chloro-3-methylpentyl (2S)-2-(6-(4′-(2-(2-(2-allyloxyethoxy)ethoxy)-ethoxy)-4-biphenylcarbonyloxy)-2-naphthyl)propionate* (**27**)

These final products were synthesized by the same method of preparing compounds (**3**, (**4**), and (**5**). The ^{1}H NMR spectra are listed in tables 4–6.

The authors would like to thank the National Science Council of the Republic of China (Contract No. NSC-84-2216-E007-029).

References

[1] Meyer, R. B., Liebert, L., Strzelecki, L., and Keller, P., 1975, *J. Phys. Lett.*, **36**, 69.
[2] Clark, N. A., and Lagerwall, S. T., 1980, *Appl. Phys. Lett.*, **36**, 898.
[3] Leslie, T. M., 1984, *Ferroelectrics*, **58**, 9.
[4] Scherowsky, G., Schliwa, A., Springer, J., Kuhnpast, K., and Trapp, W., 1989, *Liq. Crystals*, **5**, 1281.
[5] Shibaev, V. P., Kozlovsky, M. V., Plate, N. A., Bereshiev, L. A., and Blinov, L. M., 1990, *Liq. Crystals*, **8**, 545.
[6] Vallerien, S. U., Kremer, F., Fischer, E. W., Kapitza, H., Zentel, R., and Poths, H., 1990. *Makromolek. Chem. rap. Commun.*, **11**, 593.
[7] Kapitza, H., and Zentel, R., 1991, *Makromolek. Chem.*, **192**, 1859.
[8] Hsu, C. S., Shin, L. J., and Hsiue, G. H., 1993, *Macromolecules*, **26**, 3161.
[9] Chen, J. H., Chang, R. C., and Hsiue, G. H., 1993, *Ferroelectrics*, **147**, 241.
[10] Wu, S. L., Hsieh, W. J., Chen, D. G., Chen, S. J., Shy, J. T., and Hsiue, G. H., 1995, *Molec. Crystals liq. Crystals*, **265**, 39.
[11] Chen, J. H., Chang, R. C. Hsiue, G. H., Guu, F. W., and Wu, S. L., 1995, *Liq. Crystals*, **18**, 291.

[12] HSIUE, G. H., and CHEN, J. H., 1995, *Macromolecules*, **28**, 4366.
[13] CHEN, J. H., HSIUE, G. H., HWANG, C. P., and WU, J. L., 1995, *Liq. Crystals*, (in the press).
[14] HSIUE, G. H., LEE, G. R., and CHEN, J. H., 1995, *Macromolek. chem. Phys.*, **196**, 2016.
[15] KITAMURA, T., FUJII, T., and MUKOH, A., 1984, *Molec. Crystals liq. Crystals*, **108**, 333.
[16] GOODBY, J. W., WAUGH, M. A., STEIN, S. M., CHIN, E., PINDAK, R., and PATEL, J. S., 1989, *Nature (Lond.)*, **337**, 449.
[17] SLANEY, A. T., and GOODBY, J. W., 1991, *Liq. Crystals*, **9**, 849.
[18] NGUYEN, H. T., TWIEG, R. T., NABOR, M. F., ISAERT, N., and DESTRADE, C., 1991, *Ferroelectrics*, **121**, 187.
[19] DUMON, M., NGUYEN, H. T., MAUZAC, M., DESTRADE, C., ACHARD, M. F., and GASPAROUX, H., 1990, *Macromolecules*, **23**, 357.
[20] DOUCET, J., LEVELUT, A. M., LAMBERT, M., LIEBERT, L., and STRZELECK, L., 1975, *J. Phys. Colloq.*, **36**, C1–13.
[21] KOPPENHOEFER, B., and SCHURIG, V., 1987, *J. Org. Synth.*, **66**, 151.